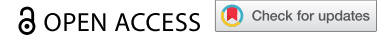


ORIGINAL RESEARCH



## MerTK-mediated efferocytosis promotes immune tolerance and tumor progression in osteosarcoma through enhancing M2 polarization and PD-L1 expression

Jinti Lin<sup>a,b</sup>, Ankai Xu<sup>a,b</sup>, Jiakang Jin<sup>a,b</sup>, Man Zhang<sup>a,b</sup>, Jianan Lou<sup>a,b</sup>, Chao Qian<sup>a,b</sup>, Jian Zhu<sup>a,b</sup>, Yitian Wang<sup>a,b</sup>, Zhengming Yang<sup>a,b</sup>, Xiumao Li<sup>a,b</sup>, Wei Yu<sup>a,b\*</sup>, Bing Liu<sup>a,b\*</sup>, and Huimin Tao<sup>a,b\*</sup>

<sup>a</sup>Department of Orthopedics, The Second Affiliated Hospital of Zhejiang University School of Medicine, Hangzhou, PR China; <sup>b</sup>Orthopedics Research Institute, Zhejiang University, Hangzhou, PR China

### ABSTRACT

The poor progress of immunotherapy on osteosarcoma patients requires deeper delineation of immune tolerance mechanisms in the osteosarcoma microenvironment and a new therapeutic strategy. Clearance of apoptotic cells by phagocytes, a process termed “efferocytosis,” is ubiquitous in tumors and mediates the suppression of innate immune inflammatory response. Considering the massive infiltrated macrophages in osteosarcoma, efferocytosis probably serves as a potential target, but is rarely studied in osteosarcoma. Here, we verified M2 polarization and PD-L1 expression of macrophages following efferocytosis. Pharmacological inhibition and genetic knockdown were used to explore the underlying pathway. Moreover, tumor progression and immune landscape were evaluated following inhibition of efferocytosis in osteosarcoma model. Our study indicated that efferocytosis promoted PD-L1 expression and M2 polarization of macrophages. Efferocytosis was mediated by MerTK receptor in osteosarcoma and regulated the phenotypes of macrophages through the p38/STAT3 pathway. By establishing the murine osteosarcoma model, we emphasized that inhibition of MerTK suppressed tumor growth and enhanced the T cell cytotoxic function by increasing the infiltration of CD8<sup>+</sup> T cells and decreasing their exhaustion. Our findings demonstrate that MerTK-mediated efferocytosis promotes osteosarcoma progression by enhancing M2 polarization of macrophages and PD-L1-induced immune tolerance, which were regulated through the p38/STAT3 pathway.

### ARTICLE HISTORY

Received 29 September 2021  
Revised 18 November 2021  
Accepted 29 December 2021

### KEYWORDS

Efferocytosis; osteosarcoma; MerTK; PD-L1; M2 polarization; immune tolerance

## Introduction

Osteosarcoma is the most frequent primary bone malignant tumor in children and adolescents, and one of the leading causes of tumor-related death in adolescents.<sup>1–3</sup> Since the 1970s, following the combined treatment of neoadjuvant chemotherapy and surgery, the therapeutic effect and prognosis of osteosarcoma have progressed greatly. Afterward, the 5-year event-free survival rate (EFS) of patients has reached 70%.<sup>4,5</sup> However, in the following decades, there has been no significant progress in the treatment of osteosarcoma. Especially in the situation where tumor recurrence, metastasis, and poor response to chemotherapy occurred on osteosarcoma patients, the overall survival rate (OS) is still less than 20%.<sup>5–7</sup> Therefore, it is urgent to explore a new treatment strategy for osteosarcoma, particularly for patients with recurrence and metastasis of osteosarcoma.


In recent years, immunotherapy has been found to be effective in various cancers.<sup>8–10</sup> For example, chimeric antigen receptor-modified T (CAR-T) cell immunotherapy has been used for treatment of malignant tumors of the lymphoid hematopoietic system,<sup>8,11</sup> and immune checkpoint therapy has become a famous strategy in a variety of malignant tumors (melanoma, non-small-cell lung cancer, breast cancer,

colorectal cancer, etc.).<sup>10,12–16</sup> Considering multiple chromosomal abnormalities and high mutation burden in osteosarcoma, immunotherapy might be a promising option.<sup>5,17</sup> However, current clinical trials of immunotherapy for osteosarcoma have not received satisfactory effects.<sup>5,18–20</sup> Thus, a new immunotherapy strategy needs to be explored.

As currently reported, macrophages are most immune cells infiltrated in the tumor microenvironment of osteosarcoma tissues and significantly related to prognosis.<sup>20–22</sup> Thus, we suspect that tumor-associated macrophages (TAM) may be a breakthrough point for immunotherapy of osteosarcoma. Clearance of apoptotic cells by phagocytes, a process termed “efferocytosis,” is a crucial function of macrophages.<sup>23,24</sup> In the physiological situation, dying cells lose the integrity of the cell membrane and intracellular contents are released, which trigger inflammation, secondary necrosis, and sometimes autoimmunity.<sup>25,26</sup> But in fact, apoptotic cells will be cleared by professional and nonprofessional phagocytes, which is termed “efferocytosis,” and the release of intracellular contents is avoided. Following efferocytosis, phagocytes release anti-inflammatory cytokines, like interleukin-10 (IL-10) and transforming growth factor- $\beta$  (TGF- $\beta$ ). Thus, efferocytosis protects tissue homeostasis from excessive inflammation and secondary

**CONTACT** Wei Yu  11818244@zju.edu.cn; Bing Liu  liubingzju@zju.edu.cn; Huimin Tao  2187040@zju.edu.cn

\*These authors contributed equally to this work.

 Supplemental data for this article can be accessed on the [publisher's website](#)

© 2022 The Author(s). Published with license by Taylor & Francis Group, LLC.

This is an Open Access article distributed under the terms of the Creative Commons Attribution-NonCommercial License (<http://creativecommons.org/licenses/by-nc/4.0/>), which permits unrestricted non-commercial use, distribution, and reproduction in any medium, provided the original work is properly cited.

necrosis.<sup>23,27</sup> However, in apoptosis-enriched tumors, the efferocytosis of TAM not only plays a role in anti-inflammation but also promotes immune tolerance in the tumor microenvironment.<sup>23,28</sup> According to published studies in breast and colon cancers, efferocytosis enhanced the release of immunosuppressive cytokines and the infiltration of myeloid-derived suppressor cells (MDSC) and Treg cells.<sup>25,29</sup> Considering the high proportion of macrophages and immunologically cold microenvironments in osteosarcoma, the relationship between efferocytosis and osteosarcoma deserves to be investigated.<sup>12,30</sup>

Moreover, tumor-associated macrophages are one of the main cell types expressing PD-L1 in the tumor microenvironment.<sup>31,32</sup> The PD-1/PD-L1 signaling pathway leads to exhaustion and functional inhibition of T cells, which is currently the main immunotherapy target.<sup>14,33,34</sup> Therefore, after efferocytosis, the PD-L1 expression on tumor-associated macrophages is worthy of attention. However, it is unclear how efferocytosis impacts the expression of PD-L1, as well as the tumor growth and immune landscape of osteosarcoma.

In this study, we explored whether efferocytosis played a substantial role in osteosarcoma growth, by evaluating its effects on M2 polarization and PD-L1 expression of macrophages, as well as on tumor progression and immune landscape in osteosarcoma. Furthermore, we conducted mechanistic studies to elucidate the mechanism by which efferocytosis regulated the phenotype of macrophages. Overall, our results suggest that MerTK-mediated efferocytosis promotes the expression of PD-L1 and the M2 polarization of tumor-associated macrophages through the p38/STAT3 pathway and enhances tumor progression and immune tolerance on osteosarcoma.

## Methods

### Antibodies and reagents

Anti-mouse monoclonal antibodies directly conjugated with fluorescein were used for flow cytometry: anti-F4/80 FITC, anti-CD11b PC7, anti-CD206 APC, and anti-CD80 PE (BD Pharmingen, USA) and anti-CD16/CD32, anti-CD45 mCHERRY, anti-CD3 FITC, anti-CD4 APCA750, anti-CD8 APC, anti-PD1 PE, anti-TIM3 PC7, and anti-CD25 BV450 (BioLegend, USA). Primary anti-mouse antibodies purchased are as follows: F4/80, Arg1, p-MerTK, and MerTK (Abcam, USA); p-p38, p38, p-STAT3, and STAT3 (Cell Signaling Technology, USA); and PD-L1 and GAPDH (Proteintech, USA). Horseradish peroxidase (HRP)-conjugated IgG secondary antibodies, 7-Amino-Actinomycin D (7AAD), and Lipofectamine 3000 were purchased from Thermo Fisher Scientific (USA). Fluorescein isothiocyanate (FITC)- and Alexa Fluor 647-conjugated IgG secondary antibodies, as well as 4',6-diamidino-2-phenylindole (DAPI) solution, were obtained from Beyotime Biotechnology (Nanjing, China). The PKH26 Red Fluorescence Cell Linker Kit was from Sigma-Aldrich (USA).

### Cell lines

RAW264.7 (a mouse leukemia virus-induced monocyte/macrophage line), K7M2 (a mouse osteosarcoma osteoblast line), NIH-3T3 (a mouse embryonic fibroblast line), and HEK-293 T (a human embryonic kidney cell line) were obtained from Procell (Wuhan, China). These cells were cultured in Dulbecco's modified eagle's medium (DMEM) supplemented with 10% fetal bovine serum (FBS, Gibco, USA) and 1% penicillin-streptomycin (P/S) and maintained in a humidified atmosphere at 37°C with 5% CO<sub>2</sub>.

### Isolation of mouse primary macrophage

BALB/c mice aged 6–8 weeks were used for isolation of primary mouse bone marrow-derived macrophages (BMDM). Cells were harvested from mouse long bones and then incubated in  $\alpha$ -minimum essential medium ( $\alpha$ -MEM) containing 30 ng/ml M-CSF (Gibco, USA), 10%FBS, and 1% P/S for 3 days. The cells were cultured in a humidified atmosphere at 37°C with 5% CO<sub>2</sub> for 5–7 days.

### In vitro efferocytosis assay

Apoptotic K7M2 cells were induced by 400  $\mu$ W/cm<sup>2</sup> ultraviolet radiation for 1 h. The apoptosis and exposure of phosphatidylserine on the cell surface were confirmed using an annexin V Apoptosis Detection Kit with PI (BioLegend). Apoptotic K7M2 cells were labeled with  $2 \times 10^{-3}$  mM PKH26 according to the kit instruction. PKH26 could label the cell membrane with red fluorescence and maintained stably during the phagocytic activity. Therefore, it was used to mark the engulfed cells. Before efferocytosis, adherent BMDMs were preincubated with 1  $\mu$ M UNC2025 for 16 h or RAW264.7 was transfected with Mer tyrosine kinase receptor (MerTK) shRNA. After apoptotic K7M2 cells were added to cocultivation for 1 h, unengulfed cells were washed away, and macrophages (BMDMs or RAW264.7) were used for further experiments.

### Plasmids, transfection, and lentiviral generation and transduction

MerTK shRNA constructs were cloned into the pLKO.1-puro vector, primer sequences of which were designed by Obio Technology (Shanghai, China), with a scramble sequence as the non-targeting control. The pLenti-puro expression vector was cotransfected with packaging vector psPAX2 and envelope vector pMD2.G into HEK-293 T cells using Lipofectamine 3000. After 16 h, transfection medium was removed and HEK-293 T cells were cultured in DMEM + 10% FBS for 48 h. Next, viruses were syringe-filtered through a 0.45- $\mu$ m filter. Then, the medium containing lentiviruses were added for infection of RAW264.7 cells with 8  $\mu$ g/mL polybrene for 48 h. Finally, successfully transfected cells were screened with puromycin and verified under a fluorescence microscope.

### Human osteosarcoma datasets and bioinformatic analysis

Raw count data of RNA-seq from osteosarcoma patients were downloaded from the TARGET project and GEO data set (GSE99671). For GSE99671, gene expression was compared to verify the difference in MerTK expression between tumors and surrounding normal tissues. For data about 88 cases of osteosarcoma patients from the TARGET project, the samples were divided into High-MerTK and Low-MerTK groups according to MerTK expression. The matrix of count values plus grouping conditions was input into DESEQ2 in R for differential analysis. Then, a table of genes with significant differential expression was output and used for gene set enrichment and pathway analysis in R, including Genome Assembly Gold-Standard Evaluations (GAGE) and Kyoto Encyclopedia of Genes and Genomes pathways (KEGG) analysis, Gene Ontology (GO) enrichment analysis and Disease Gene Network (DisGeNET) analysis, and GO enrichment analysis and Transcriptional Regulatory Relationships Unraveled by Sentence-based Text mining (TRRUST) analysis.

### Quantitative real-time polymerase chain reaction (qRT-PCR)

Trizol reagent was applied to extract total RNAs from samples. After being quantified by NanoDrop2000 (Thermo Fisher Scientific), the extracted total RNAs were used to synthesize cDNA through reverse transcription. Subsequently, qRT-PCR was performed using SYBR Premix Ex Taq II (Takara) on the ABI StepOne Plus System (Thermo Fisher Scientific). Typical cycling parameters were used as follows: 95 °C for 10 min, 40 cycles at 95 °C for 15 s, and then 60 °C for 1 min.  $\beta$ -actin was defined as internal control. The PCR for each sample was repeated three times. The  $2^{-\Delta\Delta CT}$  method was used for calculating relative expression values. Primer sequences were listed in Table S1.

### Western blotting

Cells were washed with cold phosphate buffered saline (PBS) and lysed using radio immunoprecipitation assay buffer (RIPA) supplemented with protease inhibitor and phosphatase inhibitor. Then, the extracted lysates were centrifugated, and subsequently, the supernatants were collected for quantification of protein concentration and dissolved in  $1 \times$  loading buffer. The extracted proteins were separated by sodium dodecyl sulfate-polyacrylamide gel electrophoresis (SDS-PAGE), electrotransferred onto a polyvinylidene difluoride (PVDF) membrane, and blocked with 5% nonfat milk or bovine serum albumin (BSA). Then, the membrane was incubated with the following primary antibodies overnight at 4°C: PD-L1 (1:1000), Arg1 (1:500), p-MerTK (1:500), MerTK (1:1000), p-p38 (1:1000), p38 (1:1000), p-STAT3 (1:1000), STAT3 (1:1000), and GAPDH (1:1000). After incubating with HRP-linked secondary antibodies, the protein bands were visualized by enhanced chemiluminescent (ECL) detection reagent (Fude Biologic Technology, China) under the Bio-Rad XRS chemiluminescence detection system (Hercules, CA, USA).

### Immunofluorescence staining

After engulfing apoptotic K7M2 cells, cells were washed with cold PBS, fixed with 4% paraformaldehyde, and blocked with 5% BSA. Then, the samples were incubated with anti-F4/80 (1:100) or anti-PD-L1 (1:200) primary antibodies overnight at 4°C. Subsequently, FITC- or Alexa Fluor 647-conjugated IgG secondary antibodies were incubated for 1 h, and DAPI was used for 5 min. The staining results were detected under a fluorescence microscope. This method was used to access the expression of F4/80 and PD-L1, and the efferocytosis of apoptotic K7M2 cells with PKH26 red labeling was conducted as above.

### Xenograft model mice

Male BALB/c mice aged 6–8 weeks were purchased from Shanghai SLAC Laboratory Animal Co. Ltd. and maintained under a standard condition with free fed. All protocols for animal experiments were approved by the Institutional Animal Care and Use Committee of the Second Affiliated Hospital of Zhejiang University School of Medicine (2019-No.079). Briefly, about  $5 \times 10^6$  K7M2 cells were injected subcutaneously into armpit of mice. Once the subcutaneous tumor volume reached 20 mm<sup>3</sup>, mice were treated once daily with 75 mg/kg UNC2025 or an equivalent volume of vehicle by oral gavage. Tumor burden and animal body weight were measured once every two days. Fourteen days after administration, the mice were euthanized, and the tumor samples were harvested for flow cytometry.

### Flow cytometry (FCM)

For *in vitro* FCM, after efferocytosis, RAW264.7 cells were collected, washed, and incubated with antibodies conjugated to fluorescein for 45 min at 4°C. The fluorescence was detected and analyzed using Cytexpert (v2.4, USA).

For *in vivo* FCM, tumor samples were mechanically dissected and dissociated and then digested by 1 mg/mL collagenase type IV (Gibco) and 1 mg/mL hyaluronidase (Sigma) for 45 min on a 37°C constant temperature shaker. The cell suspensions were filtered through a 70  $\mu$ m Falcon Nylon cell strainer, centrifuged, and subsequently resuspended in RBC lysis buffer (Solarbio) for 5 min. Then, the lysis buffer was neutralized and cell suspensions containing  $2 \times 10^6$  per sample were blocked with anti-CD16/CD32 antibody at 4°C for 10 min in the dark. Next, the cells were coincubated with the indicated antibodies conjugated with fluorescein for 45 min at 4°C. Finally, cells were washed with stain buffer, and fluorescence was evaluated analyzed using Cytexpert (v2.4, USA).

### Statistical analysis

Experimental data were expressed as means  $\pm$  SEM. Student's *t*-test (two-tailed, unpaired) or one-way ANOVA was applied to compare differences between groups. GraphPad Prism (v8.0; USA) and SPSS software (v20; Chicago, IL, USA) were used for statistical analysis. A *p*-value <0.05 was considered statistically significant. All experiments were repeated at least three times.



## Results

### Efferocytosis induced the M2 polarization and PD-L1 expression on macrophages

First, efferocytosis of apoptotic K7M2 cells by RAW264.7 was exhibited (Figure 1a). In the immunofluorescence, we found that the apoptotic K7M2 labeled with red appeared only in macrophages, and almost did not exist free, meaning that free apoptotic K7M2 had been cleared. To further demonstrate whether apoptotic K7M2 was washed away, we detected the CD11b and F4/80 expressions by FCM, which were markers of macrophages (Figure S1a). The result was consistent with the above judgment. Next, we evaluated the differences in gene expression of macrophages after efferocytosis. The relative mRNA expressions of M2 polarization (*Arg1*, *Il4*, and *Il10*) were significantly increased in RAW264.7 (Figure 1b, Figure S1c), and the same (*Arg1*, *Il4*, *Il10*, and *Tgfb1*) was true in BMDM (Figure 1c). The results with the apoptotic K7M2 cells as control have been exhibited to exclude the possibility of its interference (Figure S1b). Moreover, the levels of IL4 and IL10 were detected by FCM (Figure S1d). FCM showed that the percentage of CD206<sup>+</sup> macrophages (M2) was enhanced obviously after efferocytosis (Figure 1d,e). Western blot also revealed higher expression of Arg1 (Figure 1f,g). PD-L1 was a key target for tumor immunotherapy. In order to further access the effects of efferocytosis on immune function of macrophages, the expression of PD-L1 was detected. Western blot and immunofluorescence staining results demonstrated that efferocytosis increased PD-L1 expression significantly in macrophages (Figure 1f,h-j). The mRNA level of Cd274 (PD-L1) was detected (Figure S1e).

### MerTK mediated the efferocytosis of apoptotic cells by macrophage

As reported, efferocytosis was achieved in several pathways, the most common of which was through MerTK receptor. Therefore, we tried to reveal the role of MerTK in

osteosarcoma-associated efferocytosis in this study. An analysis of GEO database (GSE99671) was performed, in which RNA-seq data from the osteosarcoma group and peritumoral normal tissue group were transformed and compared (Figure 2a). The result demonstrated a significant increase of MerTK expression in osteosarcoma tissues. Tumor cells, macrophages, and fibroblasts were the most abundant cells in osteosarcoma. In order to find out which cells highly expressed MerTK in osteosarcoma tissues, the mRNA level of MerTK was compared among K7M2 (a tumor cell line), RAW264.7 (a macrophage cell line), and NIH-3T3 (a fibroblast cell line). The MerTK expression was higher significantly in RAW264.7 (Figure 2b). We inferred that it was indeed macrophages that highly express MerTK in osteosarcoma. Next, RNA-seq data from the TARGET data set were divided into High-MerTK and Low-MerTK groups, analyzed for differential expression, and functionalized by GAGE and KEGG analysis (Figure 2c). The result demonstrated that, in osteosarcoma, MerTK expression was highly correlated with several pathways including phagosome, lysosome, and endocytosis, all of which were activated during efferocytosis. Therefore, it implies that efferocytosis was induced by MerTK in osteosarcoma. Moreover, the pathway of PD-L1 expression signaling was also activated, which was in line with our result that efferocytosis promoted the PD-L1 expression in macrophages. For further experimental verification, BMDMs were administrated with MerTK inhibitor (UNC2025) and then coincubated with apoptotic K7M2 cells. It was shown that UNC2025 inhibited the efferocytosis of K7M2 by BMDMs (Figure 2d). Then, we designed shRNA (shNC, shMerTK1, shMerTK2, and shMerTK3) and transfected to RAW264.7 for MerTK knocked down (MerTK KD) (Figure 2e-g). Subsequently, we detected the efferocytosis of RAW264.7 after MerTK KD. Immunofluorescence staining showed efferocytosis was significantly attenuated in the MerTK KD group (Figure 2h,i). FCM also exhibited similar results (Figure 2j,k).

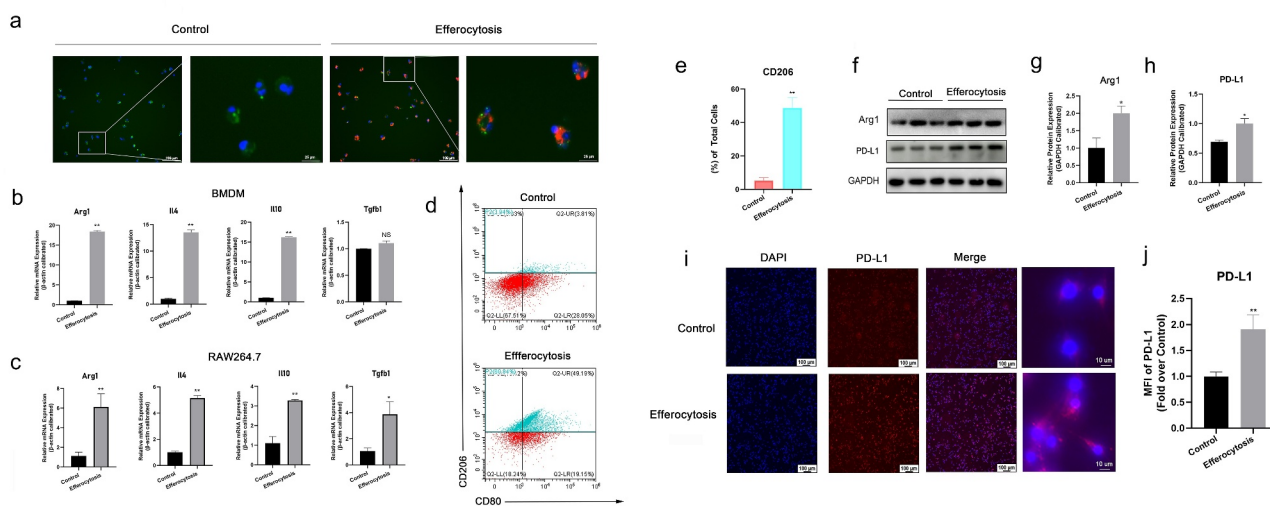


**Figure 1.** Efferocytosis induced the M2 polarization and PD-L1 expression on macrophages. (a) Efferocytosis: apoptotic K7M2 cells (red, PKH26 labeled) were endocytosed by RAW264.7 (green, F4/80 labeled). (b and c) The relative mRNA expression (*Arg1*, *Il4*, *Il10*, and *Tgfb1*) of M2 polarization in bone marrow derived macrophage (BMDM) or RAW264.7, determined by qRT-PCR. (d, e) Flow cytometry (FCM) analysis of CD206 or CD80 expression on RAW264.7. (f, g, and h) Western blot analysis and gray value analysis of Arg1, PD-L1 expression on RAW264.7, calibrated by GAPDH. (i and j) Immunofluorescence showing PD-L1 expression on RAW264.7 after efferocytosis. These results were represented as mean  $\pm$  SEM and shown as column bar graphs. \* $p < .05$ ; \*\* $p < .01$  compared to the Control group (Student's *t*-test).

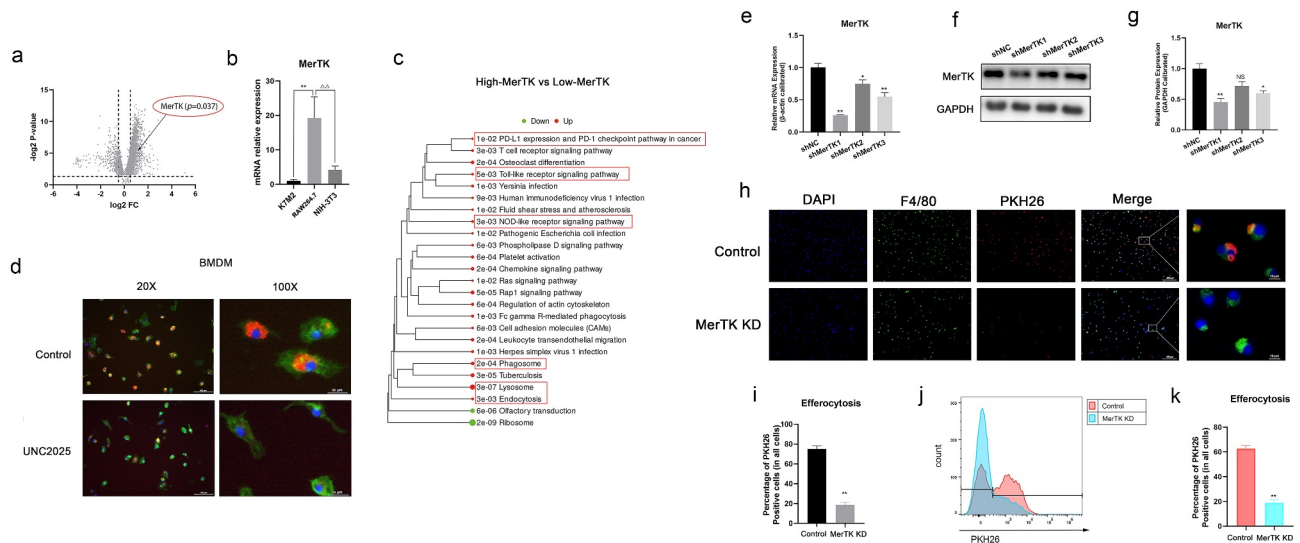


**Figure 2.** MerTK mediated the efferocytosis of apoptotic cells by macrophage. (a) Higher MerTK expression in osteosarcoma tissue than that in peritumoral normal tissues (GEO database: GSE99671). (b) The MerTK expression in K7M2 (a mouse osteosarcoma cell line), RAW264.7 (a mouse macrophage cell line), NIH-3T3 (a mouse embryonic fibroblast cell line).  $**p < .01$  compared to K7M2 group,  $\Delta\Delta p < .01$  compared to NIH-3T3 group. (c) RNA-sequencing (RNA-seq) data divided into High-MerTK and Low-MerTK groups, and functionalized by Genome Assembly Gold-Standard Evaluations (GAGE) and Kyoto Encyclopedia of Genes and Genomes pathways (KEGG) analysis (TARGET dataset). (d) Efferocytosis of apoptotic K7M2 cells (red, PKH26 labeled) by BMDM (green, F4/80 labeled) which were treated with UNC2025. (e, f, g) RAW264.7 transfected with shRNA (shNC, shMerTK1, shMerTK2, shMerTK3) and then analyzed by qRT-PCR and Western blot for MerTK expression. (h and i) Immunofluorescence showing efferocytosis of apoptotic K7M2 cells (red) by RAW264.7 (green) with shMerTK knock down (MerTK KD). (j and k) FCM analysis for efferocytosis of apoptotic K7M2 cells (PKH26 labeled) by RAW264.7 after MerTK KD. These results were represented as mean  $\pm$  SEM and showed as column bar graphs. NS meaning no significant difference,  $*p < .05$ ,  $**p < .01$ , compared to the Control group (Student's *t*-test).

**MerTK KD reversed the enhancing of PD-L1 expression and M2 polarization of macrophages induced by efferocytosis**

After verifying efferocytosis induced by MerTK in osteosarcoma, we further detected whether the increase of PD-L1 expression and M2 polarization could be reversed by MerTK KD. As a result, the mRNA expressions related to M2 polarization (*Arg1*, *Il4*, and *Il10*), which were induced by efferocytosis, were truly inhibited in the MerTK KD group (Figure 3a-c).

FCM analysis was performed to detect the intracellular protein levels of IL4 and IL10 (Figure S2a). Moreover, CD206<sup>+</sup> macrophages (M2) were decreased significantly (Figure 3d,e). Together, Western blot also showed the reduced expression of Arg1 (Figure 3f,g). Next, the PD-L1 expression were evaluated. The result of Western blot, as well as immunofluorescence staining, emphasized that the efferocytosis-induced PD-L1 expression was suppressed significantly in the MerTK KD group (Figure 3f,h-j). The mRNA expression of Cd274

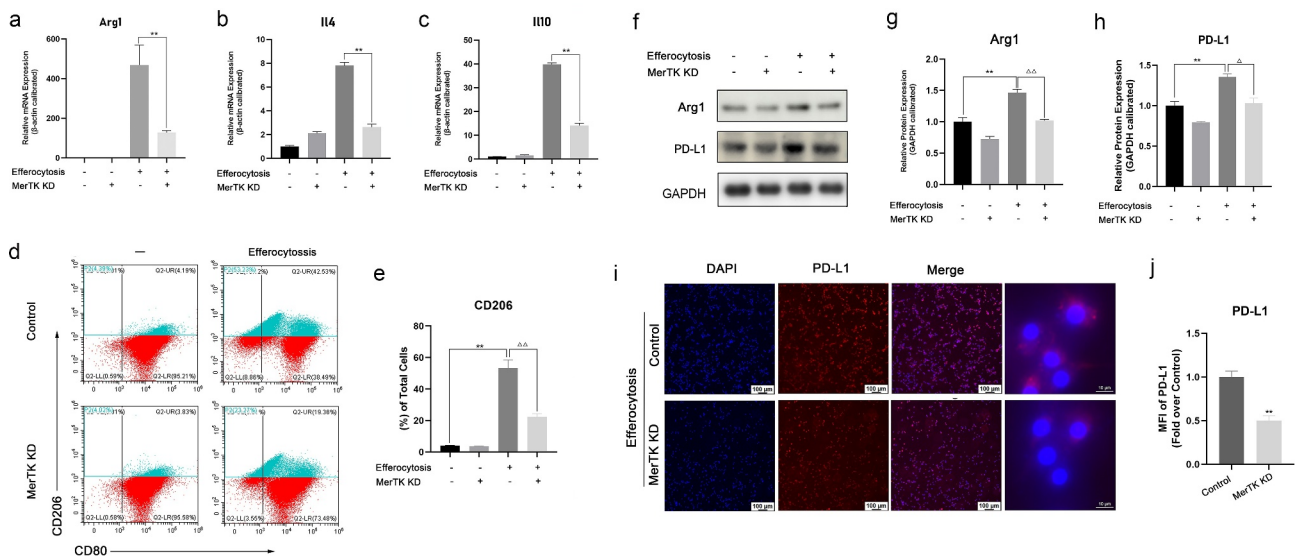


**Figure 3.** MerTK KD inhibited PD-L1 expression and M2 polarization of macrophage induced by efferocytosis. (a, b, and c) Relative mRNA expression of M2 polarization (*Arg1*, *Il4*, and *Il10*) in Control or MerTK KD group, with efferocytosis or not, analyzed by qRT-PCR. (d and e) FCM analysis of CD206 or CD80 expression. (f, g, and h) Western blot analysis and gray value analysis of Arg1 and PD-L1 expression, calibrated by GAPDH. (i and j) Immunofluorescence showing PD-L1 expression after efferocytosis. These results were represented as mean  $\pm$  SEM and shown as column bar graphs.  $\Delta p < .05$ ;  $\Delta\Delta p < .01$  compared to the MerTK KD group with efferocytosis.  $*p < .05$ ;  $**p < .01$  compared to the Control group with efferocytosis or not (Student's *t*-test).

supported the above conclusion (Figure S2b). Therefore, MerTK KD reversed the enhancing of PD-L1 expression and M2 polarization of macrophages induced by efferocytosis. And it was concluded that, in osteosarcoma, MerTK-mediated efferocytosis promoted the PD-L1 level and M2 polarization of macrophages.

### **Efferocytosis promoted PD-L1 expression and M2 polarization through the MerTK/p38/STAT3 pathway**

Next, we explored by which pathways MerTK-mediated efferocytosis regulated the function of macrophages. In the KEGG analysis of Figure 2c, we found that high-expression MerTK was followed by the activation of Toll-like receptor and NOD-like receptor signaling pathways. Together, GO enrichment analysis and DisGeNET analysis were performed for High-MerTK and Low-MerTK groups from TARGET database (Figure 4a). As a result, the correlation between inflammation and MerTK expression was the highest. Inflammation and Toll-like receptor and NOD-like receptor signaling pathways were all involved in the MAPK pathways. Therefore, we inferred that MAPK pathways might be the crucial pathway through which MerTK regulated the function of macrophages. Moreover, to find out the possible transcription factor, GO enrichment analysis and TRRUST analysis were performed (Figure 4b). It was revealed that transcription factor STAT3 was promoted significantly, which might regulate the PD-L1 expression and M2 polarization.<sup>32,35</sup>

For further verification, the expression of p-MerTK/MerTK, p-p38/p38, and p-STAT3/STAT3 was detected after 15, 30, 60, 120, and 240 min of efferocytosis. With MerTK KD, we found that the phosphorylation of p38 (p-p38/p38) and STAT3 (p-STAT3/STAT3) was inhibited significantly (Figure 4c-e), as well as the attenuated expression of PD-L1 and Arg1 (Figure 4c,f,g). Although the phosphorylation of p38 was degraded 120 min after being activated by efferocytosis, the inhibition of PD-L1 and Arg1 expression and phosphorylation of STAT3 still could be detected. Moreover, cells were administrated with p38 inhibitor (SB 203580) for 8 h. Following the phosphorylation of p38 was attenuated by SB 203580 (Figure 4h,i), the differential expression of phosphorylation of STAT3 was eliminated between Control and MerTK KD groups (Figure 4h,j). Together, the PD-L1 and Arg1 expression also was no longer depressed significantly (Figure 4h,k,l). Thus, it was emphasized that MerTK-induced efferocytosis enhanced PD-L1 expression and M2 polarization of macrophages through the p38/STAT3 pathway.

### **MerTK inhibitor (UNC2025) suppressed tumor progression in mouse osteosarcoma model**

To verify the influence of MerTK inhibition on osteosarcoma growth *in vivo*, we established a murine osteosarcoma model. The animals were treated with MerTK inhibitor (UNC2025) for 2 weeks. Tumor burden and animal body weight were measured once every two days. As a result, the tumor progression was significantly inhibited with UNC2025 administration (Figure 5a,b), and the treatment had no obvious impact on the

mouse weight (Figure 5c). Tumor growth curve for every mouse in Control and UNC2025 groups was showed by Figure 5d,e. We also compared the number of lung metastases and found that UNC2025 had no significant effect on lung metastasis (Figure 5f,g). These data indicated that the high expression of MerTK in osteosarcoma enhanced the tumor progression.

### **UNC2025 inhibited M2 polarization of macrophages and enhanced T cell cytotoxic function in mouse osteosarcoma model**

In order to evaluate the impact of MerTK inhibition on M2 polarization *in vivo*, the myeloid-focused antibody panels of FCM were used for tumor samples. The gating strategy for macrophage identification is shown in Figure 6a. The proportion of infiltrating macrophages (CD11b<sup>+</sup>F4/80<sup>+</sup>) was not obviously different in tumor microenvironment between UNC2025 and control groups (Figure 6b,d). However, the percentage of M2 (CD11b<sup>+</sup>F4/80<sup>+</sup>CD206<sup>+</sup>) macrophages were significantly reduced after UNC2025 administration (Figure 6c,e), with no difference in M1 (CD11b<sup>+</sup>F4/80<sup>+</sup>CD80<sup>+</sup>) macrophages (Figure 6c,f). The results revealed that UNC2025 depressed the M2 polarization of macrophages in osteosarcoma.

MerTK activation promoted the expression of PD-L1 in macrophages. We further investigated the relationship between MerTK expression and immunological function of osteosarcoma. FCM with lymphocyte-focused antibody panels was performed for the tumor samples. The gating strategy for lymphocyte identification was executed (Figure 6g). As a result, UNC2025 administration did not impact the infiltration of CD3<sup>+</sup> T cells in the tumor microenvironment (Figure 6h,l). Importantly, CD8<sup>+</sup> effector T cells were increased significantly (Figure 6i,m). And the PD-1<sup>+</sup>TIM3<sup>+</sup> T cells were attenuated (Figure 6j,o), meaning that UNC2025 depressed the exhausted T cells. As for CD4<sup>+</sup> T cells, no obvious impact was evaluated on the proportion of CD4<sup>+</sup> T cells (Figure 6i,n) and Treg cells (CD4<sup>+</sup>CD25<sup>+</sup>, Figure 6k,p). Thus, it could be concluded that, by increasing infiltration of CD8<sup>+</sup> T cells and suppressing exhaustion of T cells, MerTK inhibition by UNC2025 promoted immune function in osteosarcoma.

## **Discussion**

The failure of clinical trials on immunotherapy in many osteosarcoma patients emphasizes the need for a deeper understanding of the immune microenvironment of osteosarcoma and a new therapeutic strategy.<sup>5,18-20</sup> In this study, we identify that the blockade of efferocytosis by inhibiting MerTK suppressed the tumor progression and immune tolerance in osteosarcoma. Previous research studies have demonstrated that efferocytosis can promote M2 polarization of macrophages.<sup>23,26</sup> Our findings verify that efferocytosis is mediated by MerTK in osteosarcoma and promotes not only the M2 polarization of macrophages but also expression of PD-L1. Thus, MerTK probably serves as a potential target to boost immunotherapy of osteosarcoma.



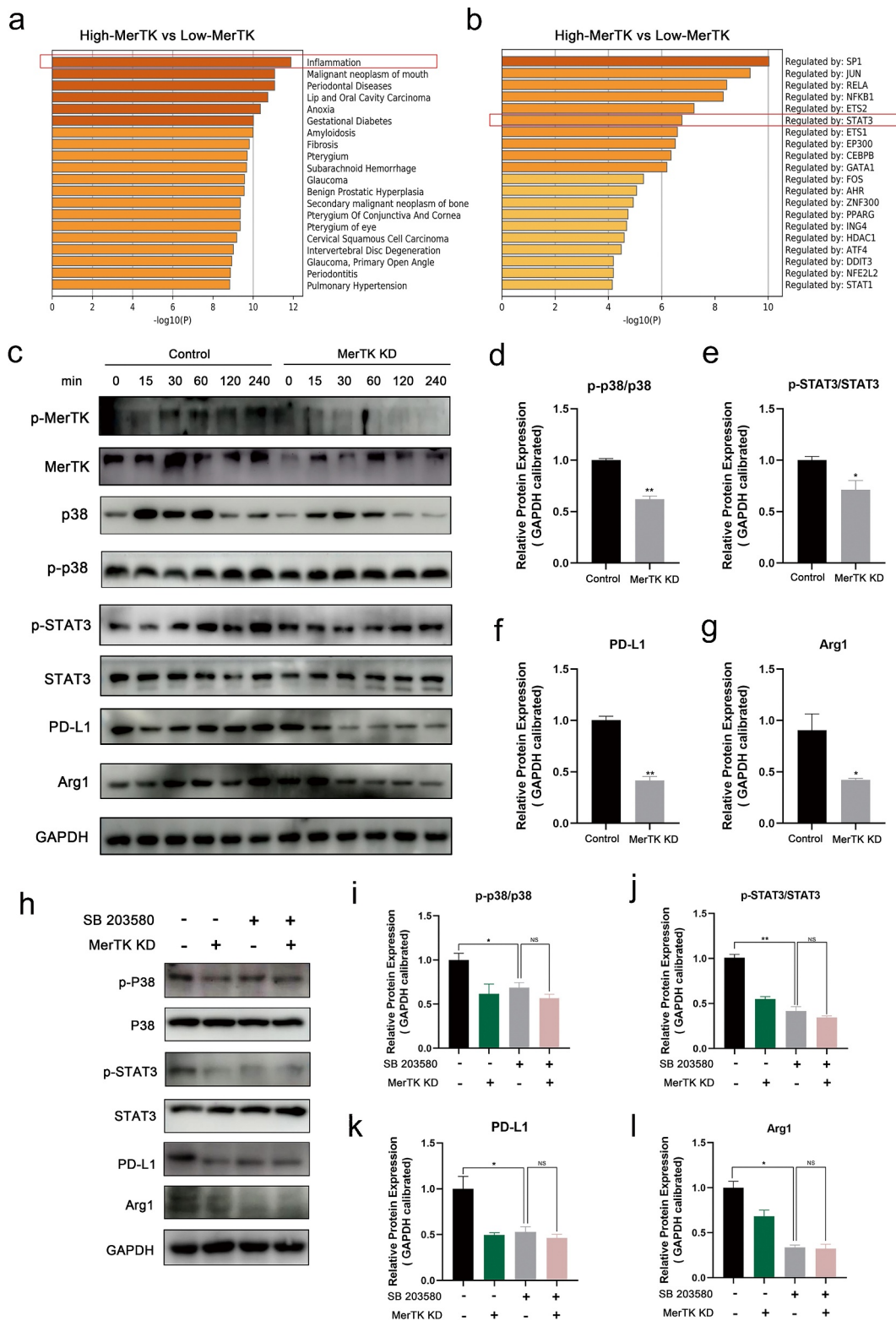


**Figure 4.** Efferocytosis promoted PD-L1 expression and M2 polarization through the MerTK/p38/STAT3 pathway. (a) RNA-seq data functionalized by Gene Ontology (GO) enrichment analysis and Disease Gene Network (DisGeNET) analysis (TARGET dataset). (b) RNA-seq data functionalized by GO enrichment analysis and Transcriptional Regulatory Relationships Unrevealed by Sentence-based Text mining (TRRUST) analysis (TARGET data set). (c) RAW264.7 transfected for MerTK KD, incubated with apoptotic K7M2 cells for 0, 15, 30, 60, 120, and 240 min, and then analyzed by Western blot for p-MerTK, MerTK, p-p38, p38, p-STAT3, STAT3, PD-L1, Arg1, and GAPDH (loading control). (d, e, f, and g) gray value analysis for Western blot (C) of PD-L1, Arg1, and the ratio of abundances of p-p38/p38, p-STAT3/ STAT3. (h) RAW264.7 transfected for MerTK KD, incubated with apoptotic K7M2 cells for 60 min, and treated with p38 inhibitor (SB 203580) or not. (i, j, k, and l) gray value analysis for Western blot (H) of PD-L1, Arg1, and the ratio of abundances of p-p38/p38, p-STAT3/ STAT3. The results were represented as mean  $\pm$  SEM and showed as column bar graphs. \* $p < .05$ ; \*\* $p < .01$ ; NS meaning no significant difference (Student's *t*-test).

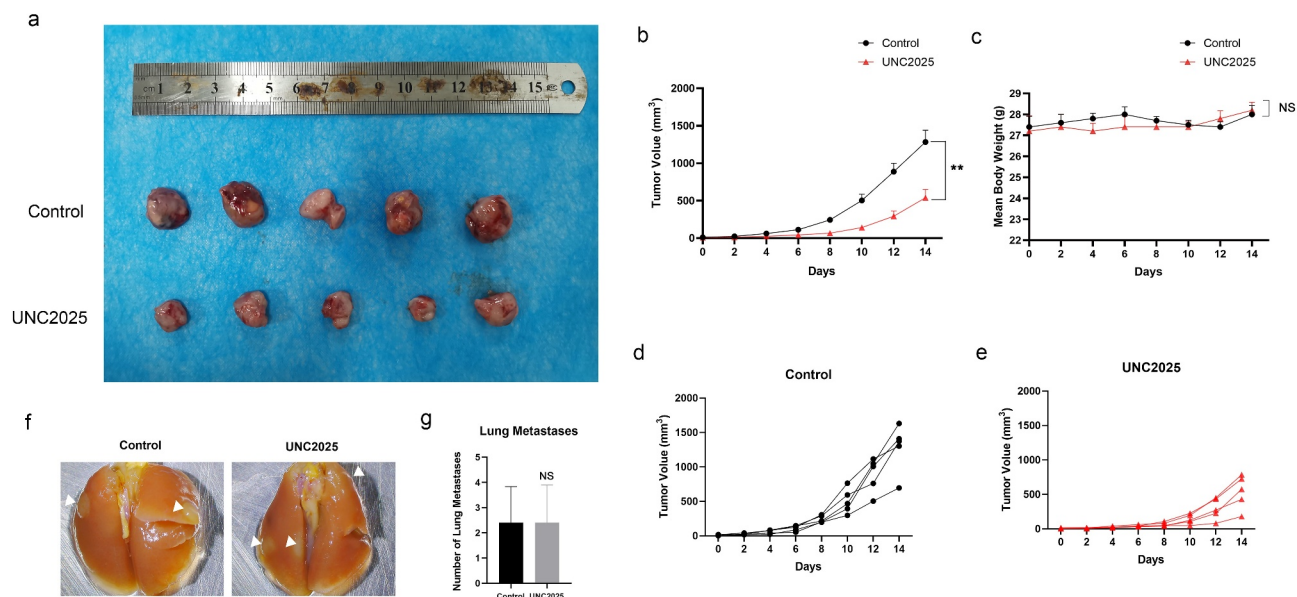


**Figure 5.** MerTK inhibitor (UNC2025) suppressed tumor progression in mouse osteosarcoma model. (a-e)  $5 \times 10^6$  K7M2 cells were injected subcutaneously into 6-week-old BALB/c mice ( $n = 5/\text{group}$ ). Mice were treated once daily with 75 mg/kg MerTK inhibitor (UNC2025) or an equivalent volume of vehicle once the subcutaneous tumor volume reached  $20 \text{ mm}^3$ . Tumor burden and animal body weight were measured once every two days. (a) tumor samples harvested in 14 days after treatment. (b and c) tumor volume and animal body weight measured once every two days when treatment. (d and e) Tumor growth curve for every mouse in Control and UNC2025 groups. (f and g) the number of lung metastases.  $**p < .01$ ; NS meaning no significant difference (Student's *t*-test).

Mechanistically, efferocytosis includes three processes: recruitment, recognition, and phagocytosis.<sup>23,36</sup> In the second process, several receptors on phagocytes recognize the signaling of apoptotic cells and then activate efferocytosis, which include MerTK, CD300 family, T cell immunoglobulin, and mucin domain containing 4 (TIM4), brain-specific angiogenesis inhibitor 1 (BAI1), and so on.<sup>23</sup> The efferocytosis in osteosarcoma has rarely been studied. We identify that macrophages recognize apoptotic osteosarcoma cells by MerTK in osteosarcoma. MerTK belongs to the receptor tyrosine kinase family (Tryo3, Axl, and MerTK), which is mainly distributed on the cell surface.<sup>26</sup> Previous papers reported that MerTK was abnormally expressed in various cancers.<sup>24,37</sup> Our data are further strengthened by analyses of several osteosarcoma patient data sets. We find that MerTK is highly expressed in osteosarcoma, and the abnormal expression of MerTK can activate pathways of phagosome, lysosome, and endocytosis, all of which are involved in the downstream of efferocytosis. MerTK has been reported as a key target of efferocytosis and immune tolerance in multiple tumors.<sup>25,29,38</sup> Compared to Tryo3 and Axl, MerTK is considered as the main receptor of efferocytosis.<sup>23,39</sup> In efferocytosis, TIM4 helps to secure apoptotic cells on phagocytes, but it cannot transduce signals by itself.<sup>40</sup>

We explored the phenotypic difference of macrophages after efferocytosis of apoptotic tumor cells and verified the increase of M2 polarization and PD-L1 expression. The former has been reported in several studies, but the latter is rarely investigated.<sup>23,26,41</sup> To further understand how efferocytosis impacts PD-L1 expression and M2

polarization, we first perform DisGeNET and KEGG analyses, which imply that MAPK (p38, ERK, and JNK) signaling cascade is activated after efferocytosis as a crucial pathway. In order to find out the possible transcription factor, TRRUST analysis was performed and showed the activation of STAT3, which can be enhanced by MerTK as reported.<sup>37,42</sup> Through mechanistic studies, we identify that MerTK-induced efferocytosis improves PD-L1 expression and M2 polarization of macrophages through the p38/STAT3 pathway. This has rarely been reported, particularly the PD-L1 expression after efferocytosis.

Therapeutically, the murine osteosarcoma model was established and UNC2025 was used *in vivo* for inhibiting MerTK.<sup>43,44</sup> The result demonstrated significant inhibition of tumor growth. Because MerTK, as the receptor of efferocytosis, can regulate the immune function of macrophages, FCM was used to evaluate the immune landscapes after UNC2025 treatment. This emphasizes that inhibiting MerTK truly suppresses the M2 polarization of TAM *in vivo*. Moreover, T cell cytotoxic function is also enhanced by increasing the total CD8<sup>+</sup> T cell number and attenuating TIM3<sup>+</sup>PD-1<sup>+</sup> exhausted CD8<sup>+</sup> T cell phenotype. We speculate that it is achieved by inhibition of PD-L1 expression and M2 polarization of macrophages. This result is consistent with previous studies in which T cell cytotoxic function was improved with Sitravatinib treatment.<sup>45</sup>

However, there are some limitations in this research. For example, the receptor tyrosine kinase family (Tryo3 and Axl) and TIM4 have not been explored in the efferocytosis of osteosarcoma. The p38/STAT3 pathway might play a role in



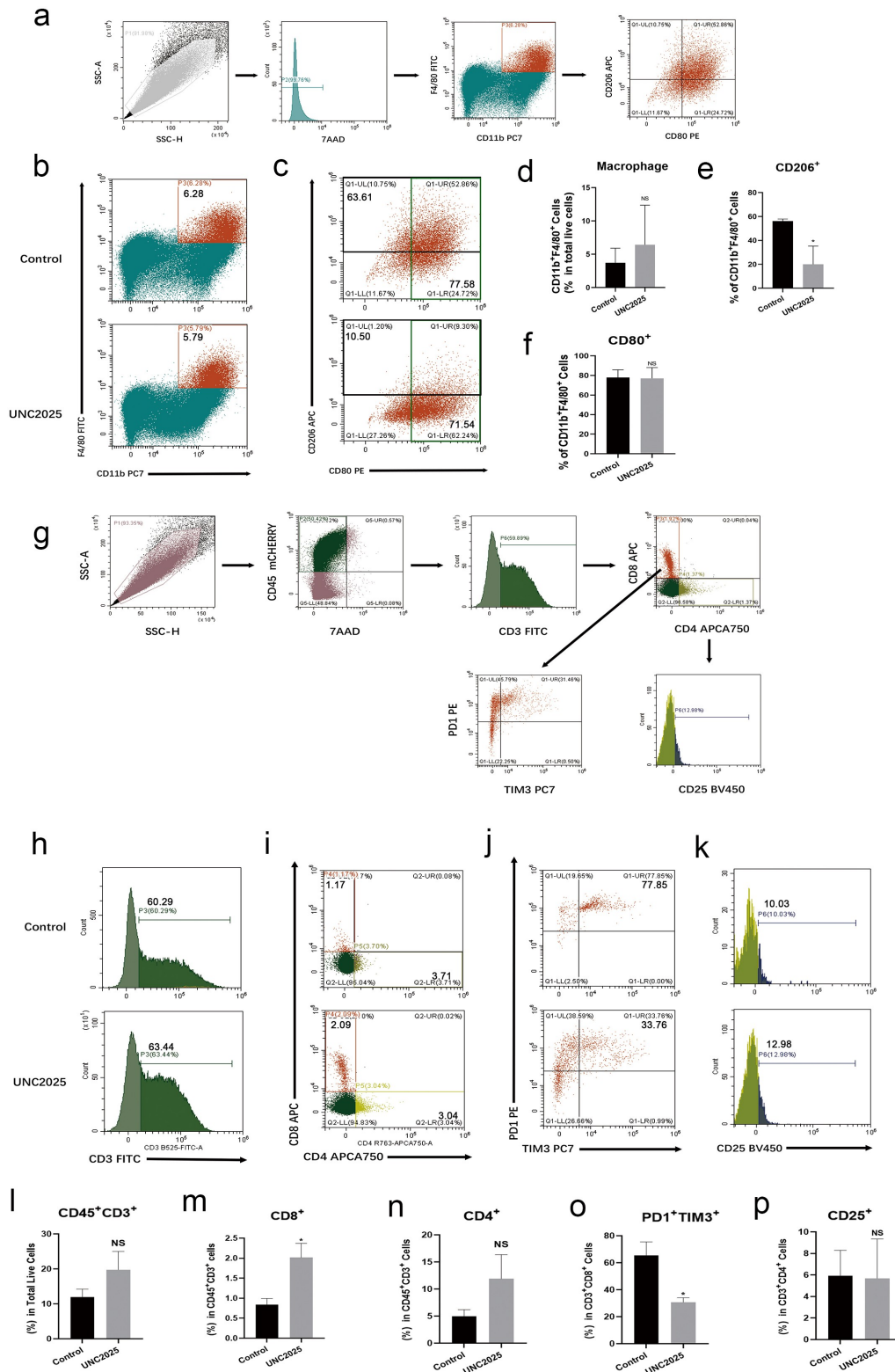


**Figure 6.** UNC2025 inhibited M2 polarization of macrophages and enhanced T cell cytotoxic function in mouse osteosarcoma model. FCM analysis of tumor-associated macrophages from the tumor single cell suspensions from mice bearing K7M2 tumors treated with UNC2025 for 14 days. (a) Gating strategy for macrophage identification using myeloid-focused antibody panels. Each data point represented a biological replicate. (b and d) The frequency of tumor-associated macrophages (CD11b<sup>+</sup>F4/80<sup>+</sup>) in the total live cells. (c, e, and f) The frequency of M2 macrophages (CD11b<sup>+</sup>F4/80<sup>+</sup>CD206<sup>+</sup>) and M1 macrophages (CD11b<sup>+</sup>F4/80<sup>+</sup>CD80<sup>+</sup>) in total CD11b<sup>+</sup>F4/80<sup>+</sup> cells. (g) Gating strategy for lymphocyte identification using lymphocyte-focused antibody panels. Each data point represented a biological replicate. (h and i) The frequency of CD45<sup>+</sup> CD3<sup>+</sup> T cells in total live cells. (j, m, and n) The frequency of CD8<sup>+</sup> T cells and CD4<sup>+</sup> T cells in CD45<sup>+</sup> CD3<sup>+</sup> T cells. (k and o) The frequency of PD-1<sup>+</sup>TIM3<sup>+</sup> T cells in CD3<sup>+</sup> CD8<sup>+</sup> T cells. (l and p) The frequency of CD25<sup>+</sup> T cells in CD3<sup>+</sup> CD4<sup>+</sup> T cells. \**p* < .05; \*\**p* < .01; NS meaning no significant difference (Student's *t*-test).

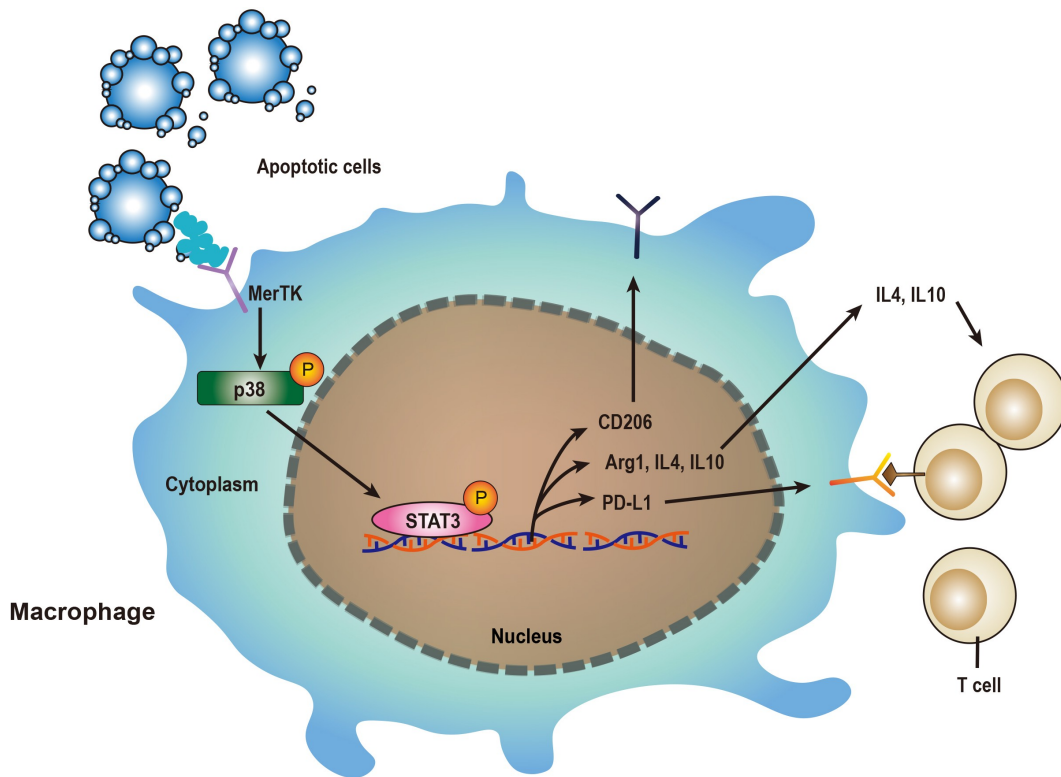


**Figure 7.** The schematic diagram: Clearance of apoptotic cells by macrophages is termed efferocytosis, which promotes the expression of PD-L1 and the M2 polarization with increased expression of Arg1, IL4, and IL10. In osteosarcoma, the process is mediated by MerTK receptor and regulates the phenotypes of macrophages through the p38/STAT3 pathway. As a result, the suppression of T cell cytotoxic function is induced.

regulation, but not the whole. We hope to explore other MerTK postreceptor signaling pathways in further research studies, like MEK, PI3K, JAK, and so on. Although pharmacological MerTK inhibition has better potential clinical value, the MerTK<sup>-/-</sup> mice have not been used to emphasize the mechanism more clearly. More detailed and systematic studies need to be investigated in the future.

## Conclusion

In summary, our study reveals that efferocytosis is mediated by MerTK in osteosarcoma and promotes the expression of PD-L1 and the M2 polarization with increased expression of Arg1, IL4, and IL10, which is regulated through the p38/STAT3 pathway. By inhibiting MerTK in *vivo*, M2 polarization of macrophages is alleviated and T cell cytotoxic function is improved; consequently, the tumor growth is suppressed (Figure 7).

## Disclosure statement

No potential conflict of interest was reported by the author(s).

## Funding

This study was supported by grants from the Natural Science Foundation of Zhejiang Province [LY18H160015 and LY20H160025] and National Natural Science Foundation of China [81872181 and 81702662].

## Authors' contributions

H. Tao and B. Liu designed conceptualization of the study, and J. Lin put it into study. A. Xu led the bioinformatic analysis. J. Jin, M. Zhang, J. Lou, and C. Qian assisted in complement of the experiment. J. Zhu and Y. Wang led data curation and analysis. J. Lin wrote the original draft. W. Yu led the design of methodology. W. Yu, X. Li, Z. Yang, H. Tao, and B. Liu reviewed the manuscript.

## References

1. Marina N. Biology and therapeutic advances for pediatric osteosarcoma. *Oncologist*. 2004;9(4):422. doi:10.1634/theoncologist.9-4-422.
2. Czarnecka AM, Synoradzki K, Firlej W, Bartnik E, Sobczuk P, Fiedorowicz M, Grieb P, Rutkowski P. Molecular biology of osteosarcoma. *Cancers (Basel)*. 2020;12(8):2130. doi:10.3390/cancers12082130.
3. Rickel K, Fang F, Tao J. Molecular genetics of osteosarcoma. *Bone*. 2017;102:69–79. doi:10.1016/j.bone.2016.10.017.
4. Anderson ME. Update on survival in osteosarcoma. *Orthop Clin North Am*. 2016;47(1):283–292. doi:10.1016/j.ocl.2015.08.022.
5. Harrison DJ, Geller DS, Gill JD, Lewis VO, Gorlick R. Current and future therapeutic approaches for osteosarcoma. *Expert Rev Anticancer Ther*. 2018;18(1):39–50. doi:10.1080/14737140.2018.1413939.
6. Endo-Munoz L, Evdokiou A, Saunders NA. The role of osteoclasts and tumour-associated macrophages in osteosarcoma metastasis. *Biochim Biophys Acta*. 2012;1826(2):434–442. doi:10.1016/j.bbcan.2012.07.003.
7. Hagleitner MM, Bont ED, Loo DT. Survival trends and long-term toxicity in pediatric patients with osteosarcoma. *Sarcoma*. 2012 Nov 25;2012:636405. doi:10.1155/2012/636405.

8. Holmström M, Hasselbalch H. Cancer immune therapy for myeloid malignancies: present and future. *Semin Immunopathol.* 2019;41(1):97–109. doi:10.1007/s00281-018-0693-x.
9. Hiam-Galvez K, Allen B, Spitzer M. Systemic immunity in cancer. *Nat Rev Cancer.* 2021;21(6):345–359. doi:10.1038/s41568-021-00347-z.
10. Billan S, Kaidar-Person O, Gil Z. Treatment after progression in the era of immunotherapy. *Lancet Oncol.* 2020;21(10):e463–e476. doi:10.1016/S1470-2045(20)30328-4.
11. Hudecek M, Lupo-Stanghellini M, Kosasih P, Sommermeyer D, Jensen M, Rader C, Riddell SR. Receptor affinity and extracellular domain modifications affect tumor recognition by ROR1-specific chimeric antigen receptor T cells. *Clin Cancer Res.* 2013;19(12):3153–3164. doi:10.1158/1078-0432.CCR-13-0330.
12. Yap T, Parkes E, Peng W, Moyers J, Curran M, Tawbi H. Development of immunotherapy combination strategies in cancer. *Cancer Discov.* 2021;11(6):1368–1397. doi:10.1158/2159-8290.CD-20-1209.
13. Eschweiler S, Clarke J, Ramírez-Suástegui C, Panwar B, Madrigal A, Chee S, Karydis I, Woo E, Alzetani A, Elsheikh S, et al. Intratumoral follicular regulatory T cells curtail anti-PD-1 treatment efficacy. *Nat Immunol.* 2021;22(8):1052–1063. doi:10.1038/s41590-021-00958-6.
14. Martinez-Usatorre A, Kadioglu E, Boivin G, Cianciaruso C, Guichard A, Torchia B, Zangger N, Nassiri S, Keklikoglou I, Schmittnaegel M, et al. Overcoming microenvironmental resistance to PD-1 blockade in genetically engineered lung cancer models. *Sci Transl Med.* 2021;13(606). doi:10.1126/scitranslmed.abd1616.
15. Damaskos C, Garpis N, Garpis A, Nikolettos K, Sarantis P, Georgakopoulou V, Nonni A, Schizas D, Antoniou EA, Karamouzis MV, et al. Investigational drug treatments for triple-negative breast cancer. *J Personalized Med.* 2021;11(7):652. doi:10.3390/jpm11070652.
16. Dutta R, Khalil R, Mayilsamy K, Green R, Howell M, Bharadwaj S, Mohapatra SS, Mohapatra S. Combination therapy of mithramycin A and immune checkpoint inhibitor for the treatment of colorectal cancer in an orthotopic murine model. *Front Immunol.* 2021;12:706133. doi:10.3389/fimmu.2021.706133.
17. Champiat S, Ferté C, Lebel-Binay S, Eggermont A, Soria J. Exomics and immunogenics: bridging mutational load and immune checkpoints efficacy. *Oncoimmunology.* 2014;3(1):e27817. doi:10.4161/onci.27817.
18. Gill J, Gorlick R. Advancing therapy for osteosarcoma. *Nat Rev Clin Oncol.* 2021;18(10):609–624. doi:10.1038/s41571-021-00519-8.
19. Paoluzzi L, Cacavio A, Ghesani M, Karambelkar A, Rapkiewicz A, Weber J, Rosen G. Response to anti-PD1 therapy with nivolumab in metastatic sarcomas. *Clin Sarcoma Res.* 2016;6(1):24. doi:10.1186/s13569-016-0064-0.
20. Gomez-Brouchet A, Illac C, Gilhodes J, Bouvier C, Aubert S, Guinebretiere J, Marie B, Larousserie F, Entz-Werlé N, de Pinieux G, et al. CD163-positive tumor-associated macrophages and CD8-positive cytotoxic lymphocytes are powerful diagnostic markers for the therapeutic stratification of osteosarcoma patients: an immunohistochemical analysis of the biopsies from the French OS2006 phase 3 trial. *Oncoimmunology.* 2017;6(9):e1331193. doi:10.1080/2162402X.2017.1331193.
21. Zhang C, Zheng J, Lin Z, Lv H, Ye Z, Chen Y, Zhang X-Y. Profiles of immune cell infiltration and immune-related genes in the tumor microenvironment of osteosarcoma. *Aging.* 2020;12(4):3486–3501. doi:10.18632/aging.102824.
22. Buddingh E, Kuijjer M, Duim R, Bürger H, Agelopoulos K, Myklebost O, Serra M, Mertens F, Hogendoorn PCW, Lankester AC, et al. Tumor-infiltrating macrophages are associated with metastasis suppression in high-grade osteosarcoma: a rationale for treatment with macrophage activating agents. *Clin Cancer Res.* 2011;17(8):2110–2119. doi:10.1158/1078-0432.CCR-10-2047.
23. Boada-Romero E, Martinez J, Heckmann BL, Green DR. The clearance of dead cells by efferocytosis. *Nat Rev Mol Cell Biol.* 2020;21(7):398–414. doi:10.1038/s41580-020-0232-1.
24. Zhou L, Matsushima G. Tyro3, Axl, MerTK receptor-mediated efferocytosis and immune regulation in the tumor environment. *Int Rev Cell Mol Biol.* 2021;361:165–210.
25. Werfel TA, Elion DL, Rahman B, Hicks DJ, Sanchez V, Gonzales-Ericsson PI, Nixon MJ, James JL, Balko JM, Scherle PA, et al. Treatment-Induced tumor cell apoptosis and secondary necrosis drive tumor progression in the residual tumor microenvironment through MerTK and IDO1. *Cancer Res.* 2019;79(1):171–182. doi:10.1158/0008-5472.CAN-18-1106.
26. Myers K, Amend S, Pienta K. Targeting Tyro3, Axl and MerTK (TAM receptors): implications for macrophages in the tumor microenvironment. *Mol Cancer.* 2019;18(1):94. doi:10.1186/s12943-019-1022-2.
27. Vago J, Amaral F, van de Loo F. Resolving inflammation by TAM receptor activation. *Pharmacol Ther.* 2021;227:107893. doi:10.1016/j.pharmthera.2021.107893.
28. Tajbakhsh A, Gheibi Hayat S, Movahedpour A, Savardashtaki A, Loveless R, Barreto G, Teng Y, Sahebkar A. The complex roles of efferocytosis in cancer development, metastasis, and treatment. *Biomedicine & Pharmacotherapy = Biomedicine & Pharmacotherapie.* 2021;140:111776. doi:10.1016/j.biopha.2021.111776.
29. Zhou Y, Fei M, Zhang G, Liang WC, Lin W, Wu Y, Piskol R, Ridgway J, McNamara E, Huang H, et al. Blockade of the phagocytic receptor MerTK on tumor-associated macrophages enhances P2X7R-dependent STING activation by tumor-derived cGAMP. *Immunity.* 2020;52(2):357–373.e9. doi:10.1016/j.immuni.2020.01.014.
30. Withers S, Skorupski K, York D, Choi J, Woolard K, Laufer-Amorim R, Sparger EE, Rodriguez CO, McSorley SJ, Monjazebe AM, et al. Association of macrophage and lymphocyte infiltration with outcome in canine osteosarcoma. *Vet Comp Oncol.* 2019;17(1):49–60. doi:10.1111/vco.12444.
31. Liu Y, Zugazagoitia J, Ahmed F, Henick B, Gettinger S, Herbst R, Schalper KA, Rimm DL. Immune cell PD-L1 colocalizes with macrophages and is associated with outcome in PD-1 pathway blockade therapy. *Clin Cancer Res.* 2020;26(4):970–977. doi:10.1158/1078-0432.CCR-19-1040.
32. Yi M, Niu M, Xu L, Luo S, Wu K. Regulation of PD-L1 expression in the tumor microenvironment. *J Hematol Oncol.* 2021;14(1):10. doi:10.1186/s13045-020-01027-5.
33. Xiong W, Zhang B, Yu H, Zhu L, Yi L, Jin X. RRM2 regulates sensitivity to sunitinib and PD-1 blockade in renal cancer by stabilizing ANXA1 and activating the AKT pathway. *Adv Sci (Weinheim, Baden-Wuerttemberg, Germany).* 2021;8:e2100881. doi:10.1002/adv.202100881.
34. Gonzalez-Ericsson P, Wulfkühle J, Gallagher R, Sun X, Axelrod M, Sheng Q, Luo N, Gomez H, Sanchez V, Sanders M, et al. Tumor-specific major histocompatibility-II expression predicts benefit to anti-PD-1/L1 therapy in patients with HER2-negative primary breast cancer. *Clin Cancer Res.* pp.5299–5306. 2021. doi:10.1158/1078-0432.CCR-21-0607
35. Bazhin AV, Von Ahn K, Fritz J, Werner J, Karakhanova S. Interferon-alpha up-regulates the expression of PD-L1 molecules on immune cells through STAT3 and p38 signaling. *Front Immunol.* 2018;9:2129. doi:10.3389/fimmu.2018.02129.
36. Morioka S, Maueröder C, Ravichandran K. Living on the edge: efferocytosis at the Interface of Homeostasis and Pathology. *Immunity.* 2019;50(5):1149–1162. doi:10.1016/j.immuni.2019.04.018.
37. Huelse J, Fridlyand D, Earp S, DeRyckere D, Graham D. MERTK in cancer therapy: targeting the receptor tyrosine kinase in tumor cells and the immune system. *Pharmacol Ther.* 2020;213:107577.



38. Stanford JC, Young C, Hicks D, Owens P, Williams A, Vaught DB, Morrison MM, Lim J, Williams M, Brantley-Sieders DM, et al. Efferocytosis produces a prometastatic landscape during postpartum mammary gland involution. *J Clin Invest.* 2014;124(11):4737–4752. doi:10.1172/JCI76375.
39. Doran AC, Yurdagul A Jr., Tabas I. Efferocytosis in health and disease. *Nat Rev Immunol.* 2020;20(4):254–267. doi:10.1038/s41577-019-0240-6.
40. Cunha LD, Yang M, Carter R, Guy C, Harris L, Crawford JC, Quarato G, Boada-Romero E, Kalkavan H, Johnson MDL, et al. LC3-associated phagocytosis in myeloid cells promotes tumor immune tolerance. *Cell.* 2018;175(2):429–441 e416. doi:10.1016/j.cell.2018.08.061.
41. Graham DK, DeRyckere D, Davies KD, Earp HS. The TAM family: phosphatidylinositol sensing receptor tyrosine kinases gone awry in cancer. *Nat Rev Cancer.* 2014;14(12):769–785. doi:10.1038/nrc3847.
42. Eom H, Kaushik N, Yoo K, Shim J, Kwon M, Choi M, Yoon T, Kang S-G, Lee S-J. MerTK mediates STAT3-KRAS/SRC-signaling axis for glioma stem cell maintenance. *Artif Cells Nanomed Biotechnol.* 2018;46:87–95. doi:10.1080/21691401.2018.1452022.
43. DeRyckere D, Lee-Sherick AB, Huey MG, Hill AA, Tyner JW, Jacobsen KM, Page LS, Kirkpatrick GG, Eryildiz F, Montgomery SA, et al. UNC2025, a MERTK small-molecule inhibitor, is therapeutically effective alone and in combination with methotrexate in leukemia models. *Clin Cancer Res.* 2017;23(6):1481–1492.
44. Zhang W, DeRyckere D, Hunter D, Liu J, Stashko MA, Minson KA, Cummings CT, Lee M, Glaros TG, Newton DL, et al. UNC2025, a potent and orally bioavailable MER/FLT3 dual inhibitor. *J Med Chem.* 2014;57(16):7031–7041. doi:10.1021/jm500749d.
45. Du W, Huang H, Sorrelle N, Brekken RA. Sitravatinib potentiates immune checkpoint blockade in refractory cancer models. *JCI Insight.* 2018;3(21). doi:10.1172/jci.insight.124184.